# ESTIMATION OF REFLECTIVE PROPERTIES FROM LIGHT CURVES OF A H2A ROCKET BODY

**A.Vananti[(1)], D. Guthruf[(1)], Y. Lu[(1)(2)], T. Schildknecht[(1)]**

*[(1)] Astronomical Institute, University of Bern, Sidlerstrasse 5, 3012 Bern, Switzerland, Email: alessandro.vananti@aiub.unibe.ch, guthrufdaniel@gmail.com, thomas.schildknecht@aiub.unibe.ch*
*[(2)] Chinese Academy of Sciences, Purple Mountain Observatory, Nanjing, China, Email: yaoluastro@gmail.com*

## ABSTRACT

Information about the attitude motion of space debris is mostly crucial for active debris removal missions and in case of contingencies. One technique available to characterize the attitude of space objects consist in acquiring photometric measurements thereof over time. The variation of the apparent brightness as a function of time is represented in a so-called light curve. From this time series, information about the object's attitude can be extracted. In simple cases the light curve exhibits a clear periodic variation and it can be deduced that the object rotates around some axis with a certain angular velocity. More difficult cases do not show a clear pattern and only allow a qualitative information. In few situations the approximate knowledge of the object shape gives the possibility to characterize its rotation axis in the body-fixed frame.
This paper focuses on the analysis of one space object in particular. The observed debris target is a rocket body of the type H2A. The light curves in this case show a characteristic double peak, which gives additional information about the orientation of the rocket body in the inertial frame. Furthermore, based on the relative intensity of several features within the light curve, the reflective properties of different parts of the object can be refined by comparison with simulated measurements.

## 1 INTRODUCTION

One of the solutions proposed to face the growing problem of orbital debris is active debris removal (ADR). This approach has to be taken into account to remove large-mass objects like disposed upper stages or big satellites, and stabilize or reduce the future debris population. The knowledge of the attitude state of the candidate is crucial for the mission and for the choice of the removing approach. The same applies in contingency situations, where the affected satellite is not responsive any longer and any information, included the attitude state, can be useful to understand the problem. While for operational satellites the attitude state can be deduced from telemetry data, for debris objects different observation techniques like photometric measurements, laser ranging, and radar data are used.
In the photometric measurements the variation of the brightness of the object over time, also called light curve, provides information about the rotation of the observed object. Several studies were performed to extract debris rotation rates from light curves [1][2][3]. The combination of light curves and Satellite Laser Ranging (SLR) data was used to derive spin period and analyze the temporal evolution of space debris in [4][5]. Kirchner et al. [7] combined so-called single-photon light curves and SLR measurements for the same purpose. In [6] multiple methods (passive optical, SLR, radar) are used for validation and refinement of the attitude state. The spin axis orientation of defunct satellites equipped with retroreflectors was identified in several works [8][9][10]. Santoni et al. [12] determined from light curves the direction of the rotation axis of a rocket body (R/B). Their approach, also called "amplitude method" is based on the ratio of the maximal and minimal brightness extracted from the light curve. In [13] with a similar approach, the authors were able to estimate in addition to the spin axis of a rocket body also its precession motion. A different approach for attitude determination is the so-called "epoch method" described in [14][15]. Recently, Zhao et al. were able to deduce the attitude parameters of a rocket body combining the epoch method and a procedure based on the fitting of residuals from light curves and SLR measurements [11].
In this work, light curves of a H2A rocket body are analysed to retrieve the possible direction of the angular velocity vector and to refine the reflective properties of the different components. Here a new method to determine the attitude is used, based on a characteristic of the light curves, which regularly show pronounced peaks. After the orientation of the rocket body is identified, the reflective properties are refined comparing with light curves simulations.

## 2 ATTITUDE DETERMINATION

The analyzed H2A rocket body (2010-045B) flies on an eccentric orbit with apogee at 15'683 km, perigee at 182 km, and inclination around 32°. This second stage exhibits a conical surface, whose inclination can be characterized by an angle $\theta_s$ (see Figure 1). The indicated angle of 47° is simply measured from the schematic picture of the object [16]. Due to the conical surface the light curves show characteristic peaks at regular time intervals corresponding to geometric

conditions with specular reflection (Figure 2). The intervals are related to the rotation of the body w.r.t. the Sun and the observer. In the following a method is described which was proposed by Y. Lu in 2019 to determine the rotational axis of the body.

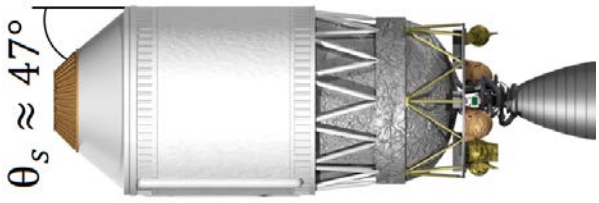


Figure 1: H2A rocket body (2010-045B).

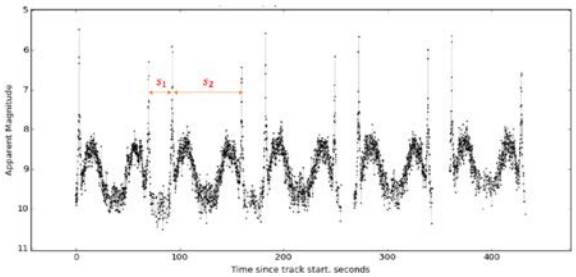


Figure 2: Light curve of H2A rocket body.

In Figure 3 the origin of the reference system corresponds to the center of mass of the R/B and the *Z* axis is the phase angle bisector. Here the lines passing by the origin and showing a specific direction are represented by their intersection points with the unit sphere.

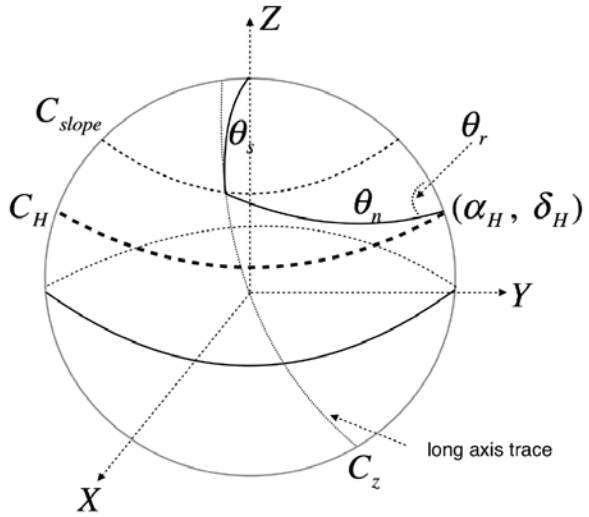


Figure 3: Scheme showing the angular momentum direction $(\alpha_H, \delta_H)$ w.r.t. the phase angle bisector *Z*.

The direction of the angular momentum *H* is then described in spheric coordinates with zenith angle $\theta_H = \frac{\pi}{2} - \delta_H$ and azimuthal angle $\alpha_H$. For angular momenta directions $(\alpha_H, \delta_H)$ on the latitude line $C_H$ the same reflection conditions apply, being the zenith angle $\theta_H$ w.r.t. the phase angle bisector *Z* constant. The angle $\alpha_H$ remains unconstrained.

The latitude line $C_{slope}$ shows the possible directions of the symmetry axis *z* of the cone that satisfy specular reflection, namely when there is a plane tangent to the cone which is perpendicular to the phase angle bisector *Z*. The zenith angle which indicates this latitude is equal to the angle $\theta_s$ related to the cone aperture.

The line $C_z$ shows the possible directions of the *z* axis of the tumbling body according to a given *H*. In fact $C_z$ lies in a plane perpendicular to the direction $(\alpha_H, \delta_H)$ and can be seen as a latitude line w.r.t. $(\alpha_H, \delta_H)$, expressed by a zenith angle $\theta_n$. The latter is 90° in case of flat spin, but can diverge if a nutation motion is present. In the following the angle $\theta_n$ will be referred as nutation angle.

The intersection of $C_{slope}$ and $C_z$ is the orientation which satisfies specular reflection for a given *H* and $\theta_n$. From this intersection point a spherical triangle with the sides $\theta_s$, $\theta_n$, and $\theta_H$ can be constructed. Here is $\theta_r$ the rotation angle of the cone *z* axis around *H* starting at the position in which *z*, *Z*, and *H* are coplanar. If we imagine $C_z$ as a latitude line w.r.t. the pole *H*, then is $\theta_r$ the azimuthal angle of *z*. An equivalent specular reflection condition can be found at an angle $-\theta_r$ in the opposite position w.r.t. the *Y*-*Z* plane.

The two peaks in the light curve in Figure 2, separated by the interval $s_1$ correspond to the orientations at $-\theta_r$ and $\theta_r$. With $s_1 + s_2 = 2\pi$ and $s_1 = 2\theta_r$ we have:

$$\frac{s_1}{s_2} = \frac{\theta_r}{\pi - \theta_r}. \qquad (1)$$

Thus $\theta_r$ can be obtained from the measurements and given $\theta_s$, $\theta_n$, and $\theta_r$, the angle $\delta_H$ can be calculated applying the spherical triangle cosine formula and substituting $\theta_H$ with $\frac{\pi}{2} - \delta_H$:

$$\cos\theta_s = \cos\theta_r \sin\theta_n \cos\delta_H + \sin\delta_H \cos\theta_n \qquad (2)$$

The angles $\theta_s$ and $\theta_r$ are per definition in the interval $[0, \frac{\pi}{2}]$ while $\delta_H$ accepts values in the interval $[-\frac{\pi}{2}, \frac{\pi}{2}]$. The eq. (2) does not have for any combination of angles a real solution. In those cases where the equation is solvable, two real solutions occur due to the ambiguity of the cosine:

$$\delta_H = \pm \operatorname{acos}\frac{\cos\theta_s}{R} + \beta \qquad (3)$$

where

$$R = \sqrt{a^2 + b^2} \qquad (4)$$

$$\beta = \operatorname{atan}\frac{b}{a} \qquad (5)$$

$$a = \cos\theta_r \sin\theta_n \qquad (6)$$

$$b = \cos\theta_n. \qquad (7)$$

For a nutation angle $\theta_n$ = 90° it is easy to see that the two solutions are symmetric angles $\pm\delta_H$, which reflect the ambiguity in the sense of rotation of the body. However, for $\theta_n$ < 90° the two solutions are on different rotation axes. In this case for further disambiguation not only the position of the peaks has to be considered but also the shape of the light curve characterized by diffuse reflection. Even if $\delta_H$ can be restricted to one solution the value of $\alpha_H$ is still not known. To further constrain the problem another light curve is necessary providing a new $\delta'_H$ value w.r.t. another phase angle bisector $Z'$. The intersection of the two circles $C_H$ and $C'_H$ in the inertial system provides two common solutions for the object. These are symmetric w.r.t. the plane defined by the two bisectors and correspond to symmetric reflection conditions. Figure 4 shows the intersection of different circles in inertial frame computed from light curves of the same object. The mirrored conditions due to the ambiguity in $\delta_H$ are omitted in this figure. In this example the intersections indicate still two possible solutions. To constrain the problem to a unique solution additional measurements are required with bisectors not coplanar to the existing ones. If additional observations are not available the overall shape of the light curve can be considered, where the solution with the best fit is selected. Alternatively, considering the motion of the angular momentum over few days can help identify a unique solution. However, these alternative constraints do not always lead to disambiguation.

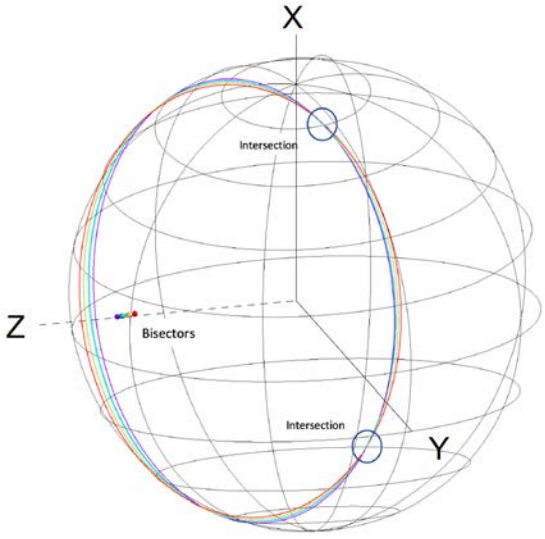


Figure 4: Circles $C_H$ and phase angle bisectors from different light curves of the same object shown in inertial frame.

## 3 FITTING OF LIGHT CURVES

Four different light curves of the H2A rocket body (2010-045B) were analyzed. Part of the light curves, in the period between 2016 and 2019, were acquired with the 1-meter Zimmerwald Laser and Astrometry Telescope (ZIMLAT) at the Swiss Optical Ground Station and Geodynamics Observatoy Zimmerwald, Switzerland. Other were available in the database of the Mini-Mega-TORTORA Wide Angle Surveillance System [18]. The measured light curves were compared to simulations to characterize unknown properties of the rocket body.

For the determination of the rotation axis the method described in the previous section was used. We assumed that the attitude of the body was already in flat spin state with a nutation angle $\theta_n$ = 90°. With the available observations it was not possible to solve the ambiguity in the angular momentum. Also alternative constraints based on the light curve shape or motion of the angular momentum mentioned before were not successful. However, the light curves simulated assuming the different possible solutions for the angular momentum exhibit almost no difference. Thus, an analysis of the optical properties based on light curve characteristics can anyway be conducted.

In the simulations we assumed a simplified model with four different components (see Figure 5): Top, Cone, Cylinder, and Bottom. For the cylinder part we assumed height 9.2 m and diameter 4 m [16]. Regarding the optical properties we adopted the Cook-Torrance model for the Bidirectional Reflectance Distribution Function (BRDF) [17]. The model defines: specular coefficient $s$, diffuse coefficient $d$ (where $s + d = 1$), diffuse albedo $\omega$, and surface roughness $m$.

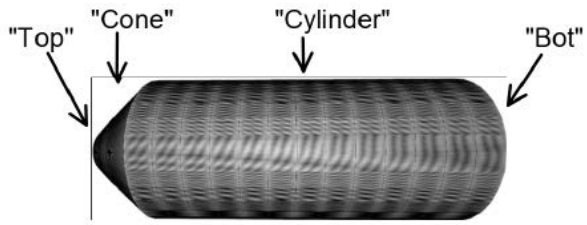


Figure 5: Simplified model of H2A rocket body.

### 3.1 Effect of parameter variation

Before comparing with the real measurements preliminary simulations were performed to characterize the influence of the different parameters. From the simulations it is visible that the single components of the object roughly determine the shape of specific parts of the light curve. Referring to Figure 6 the light curve can be divided in characteristic sections: peak, hill, spike, valley. Since the peaks are related to the cone, the following hill section consequently corresponds to the cylinder, while the spike is caused by the bottom part. The valley between the peaks is attributed to the top component. Variations in the reflection properties of the different components affect prevalently the intensity of the corresponding light curve section, as illustrated from Figure 7 to Figure 10. Here, examples of light curve simulations are shown where one selected optical

property is varied in one particular object component. The intensity is indicated on a relative magnitude scale.

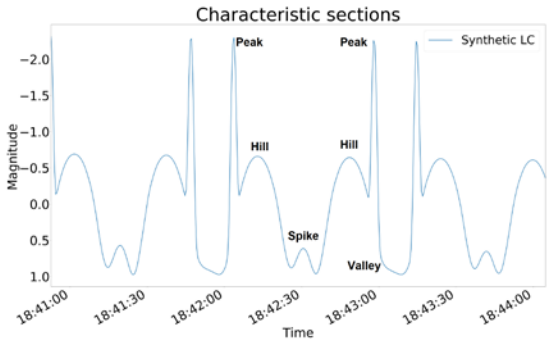


Figure 6: Characteristic sections of the light curve.

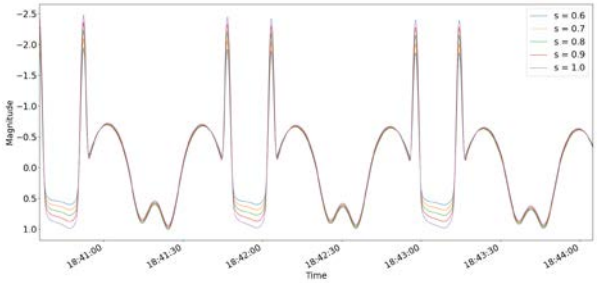

Figure 7: Simulated light curves with different specular coefficients *s* for the Cone component.

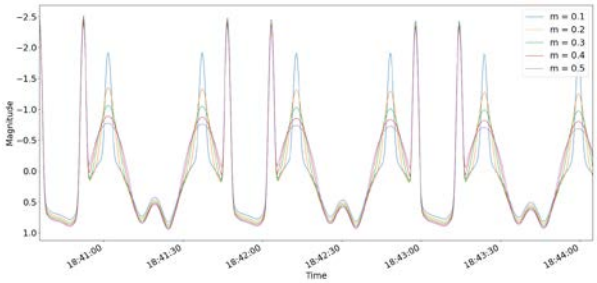

Figure 8: Simulated light curves with different surface roughness values *m* for the Cylinder component.

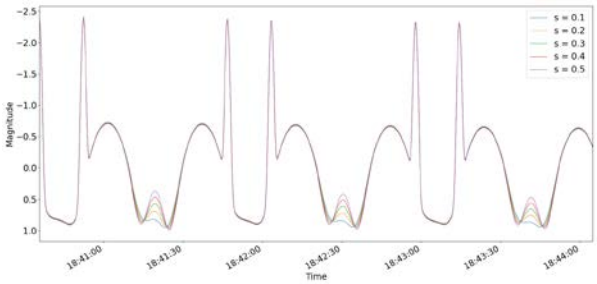

Figure 9: Simulated light curves with different specular coefficients *s* for the Bottom component.

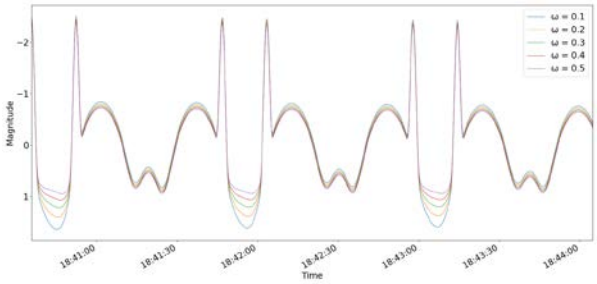

Figure 10: Simulated light curves with different diffuse albedo values $\omega$ for the Top component.

### 3.2 Estimation of optical properties

The optical properties of the four components were estimated by means of a least squares procedure using measured and simulated data. The measurements were resampled and interpolated to the simulated intervals of 0.1 s. Before applying the least squares algorithm a rough delimitation of the search space with a coarse grid of values was performed. This part is referred later as "brute force" fit (BF-fit). Due to the large number of parameters to be estimated and the consequent large computation time, the parameter estimation was applied on the single object components separately. This neglects in first approximation the cross correlation between the different components, i.e. the fact that varying e.g. one optical coefficient for the cylinder affects not only the corresponding hill section, but also the other sections of the light curve. Figure 11 and Figure 12 show observations from two different nights and the light curves simulated with the estimated parameters. With different colors, simulations are illustrated with the parameters after the brute force fit (BF-Fit) and the least squares fit (LS-Fit). Also indicated in the upper left part are the Pearson correlation coefficients [19] for the two cases as a measure for the goodness of the fit. In general, from the figures we see that the intensity of the peak is underestimated in the simulations. This is a consequence of the fact that the peaks are quite sharp and the adopted resolution for the simulations results to be too low to describe them.

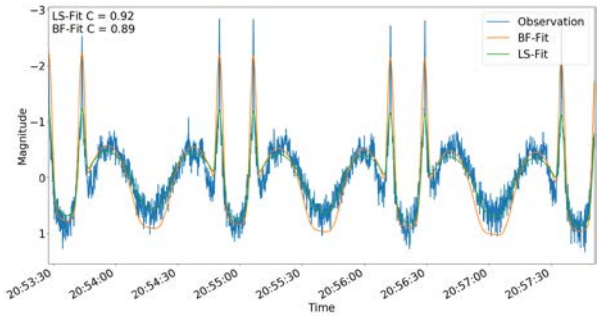


Figure 11: Real and simulated light curves of H2A rocket body. Observation from 2018-08-23.

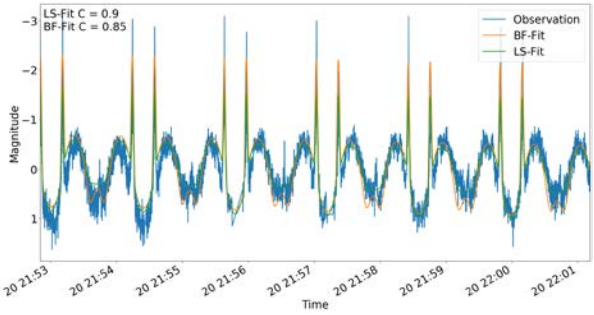


Figure 12: Real and simulated light curves of H2A rocket body. Observation from 2018-09-22.

In Table 1 the average values of the optical coefficients of the different components, computed from the four observations, and their standard deviations are indicated. Here, it has to be reminded that variations of different optical coefficients partially result in similar effects in the light curve, as was shown in Figure 7 to Figure 10. This means that the coefficients are quite correlated. In addition, as previously mentioned, in the parameter estimation the object components were treated separately. Due to the above reasons, the found coefficients have to be considered as a rough estimate.

| | *s* | Std. | *m* | Std. | ω | Std. |
|---|---|---|---|---|---|---|
| Cone | 0.952 | 0.013 | 0.065 | 0.011 | 0.122 | 0.027 |
| Top | 0.080 | 0.026 | 0.650 | 0.000 | 0.587 | 0.130 |
| Cylinder | 0.217 | 0.042 | 0.678 | 0.046 | 0.384 | 0.092 |
| Bottom | 0.200 | 0.060 | 0.285 | 0.170 | 0.327 | 0.018 |

Table 1. Average values of the optical coefficients and their standard deviation.

## 4 CONCLUSIONS

Light curves of a H2A rocket body were analysed to determine its attitude motion and to extract its optical properties. A new approach to extract the attitude information was applied. The method is based on the specular reflection conditions of the conical surface of the rocket body. Several light curves are required to uniquely determine the spin axis of the body. Alternatively, other features present in the light curves can be exploited to disambiguate the possible rotation axes. In a second step, measured and simulated light curves were considered for a least squares approach to extract reflective coefficients of different parts of the object. The intensity in different sections of the light curves is prevalently determined by specific components of the rocket body. As an approximation, the latter were considered separately in the estimation of the optical properties. On the other hand, it was noted that the estimated optical parameters are highly correlated. This is visible in the simulations, where same effects in the light curves can be obtained with different combinations of coefficients. Nonetheless, the estimate shows consistent indicative values for the optical characteristics of the rocket body.

## 5 REFERENCES

1. Earl, M.A., Wade, G.A., Observations and analysis of the apparent spin period variations of inactive boxwing geosynchronous resident space objects, Proceedings of 65th International Astronautical Congress, Toronto, Canada, 2014

2. Dearborn, M., Tippets, R., Chun, F.K., et al., Spin-axis determination of SL-8 second stage rocket bodies, Proceedings of 63rd International Astronautical Congress, Naples, Italy, 2012

3. Silha, J., Pittet, J.N., Hamara, M., Schildknecht, T., Apparent rotation properties of space debris extracted from photometric measurements, Advances in Space Research, 61, 2018

4. Schildknecht, T., Linder, E., Silha, J., Hager, M., Koshkin, N., Korobeinikova, E., Melikiants, S., Shakun, L., Strakhov, S., Photometric monitoring of non-resolved space debris and databases of optical light curves, Proceedings of AMOS Advanced Maui Optical and Space Surveillance Technologies Conference, Maui, Hawaii, US, 2015

5. Schildknecht, T., Silha, J., Pittet, J.N., Rachman A., Attitude states of space debris determined from optical light curve observations, Proceedings of 1st IAA Conference on Space Situational Awareness (ICSSA), Orlando, Florida, US, 2017

6. Schildknecht, T., Determining, Monitoring, and Modelling the Attitude Motion of Potential ADR Targets, Clean Space Industrial Days, ESA/ESTEC, Noordwijk, Netherlands, 2016

7. Kirchner, G., Steindorfer, M., Wang, P., Koidl, F., Kucharski, D., Silha, J., Schildknecht, T., Krag, H., Flohrer, T., Determination of attitude and attitude motion of space debris using laser ranging and single-photon light curve data, Proceedings of 7th European Conference on Space Debris, ESA/ESOC, Darmstadt, Germany, 2017

8. Kucharski, D., Kirchner, G., Koidl, F., Fan, C., Carman, R., Moore, C., Dmytrotsa, A., Ploner, M., Bianco, G., Medvedskij, M., Attitude and spin period of space debris Envisat measured by Satellite Laser Ranging, IEEE Transactions on Geoscience and Remote Sensing, 52, 2014

9. Kucharski, D., Lim, H.C., Kirchner, G., Hwang, J.Y., Spin parameters of LAGEOS-1 and LAGEOS-2 spectrally determined from Satellite Laser Ranging data, Advances in Space Research, 52, 2013

10. Pittet, J.N., Silha, J., Schildknecht, T., Spin motion

determination of the Envisat satellite through laser ranging measurements from a single pass measured by a single station, Advances in Space Research, 61, 2018

11. Zhao, S., Steindorfer, M., Kirchner, G., Zheng, Y., Koidl, F., Wang, P., Shang, W., Zhang, J., Li, T., Attitude analysis of space debris using SLR and light curve data measured with single-photon detector, Advances in Space Research, 65, 2020

12. Santoni, F., Cordelli, E., Piergentili, F., Determination of disposed-upper-stage attitude motion by ground-based optical observations, Journal of Spacecraft and Rockets, 50, 2013

13. Yanagisawa, T., Kurosaki, H., Shape and motion estimate of LEO debris using light curves, Advances in Space Research, 50, 2012

14. Hall, D., Africano, J., Archambeault, D., Birge, B., Witte, D., Kervin, P., AMOS observations of NASA's IMAGE satellite, Proceedings of AMOS Advanced Maui Optical and Space Surveillance Technologies Conference, Maui, Hawaii, US, 2006

15. Hall, D., Kervin, P., Optical characterization of deep-space object rotation states, Proceedings of AMOS Advanced Maui Optical and Space Surveillance Technologies Conference, Maui, Hawaii, US, 2014

16. Japan Aerospace Exploration Agency, About H-IIA Launch Vehicle, 2015, https://global.jaxa.jp/projects/rockets/h2a/index.html

17. Blacketer, L.D.J., Lewis, H.G., Urrutxua, H., Quantifying the response of a synthetic light curve generation model to varying iniputs, AMOS Advanced Maui Optical and Space Surveillance Technologies Conference, Maui, Hawaii, US, 2018

18. Karpov, S., Katkiva, E., Beskin, G., Biryukov, A., Bondar, S., Davydov, E., Ivanov, E., Perkov, A., Sasyuk, V., Massive photometry of low-altitude artificial satellites on Mini-Mega-TORTORA, Proceedings of IV Workshop on Robotic Autonomous Observatories, Revista Mexicana de Astronomia y Astrofisica, 48, 2016

19. Prabhakara, G.N., Pearson's Correlation, In: Biostatistics, JAIPEE, p. 180, 2006